Research Square

Preprints are preliminary reports that have not undergone peer review.
They should not be considered conclusive, used to inform clinical practice,
or referenced by the media as validated information.

First-principles investigation of pressure-dependent structural, electronic, vibrational, and thermodynamic properties of zinc-blende CdTe under hydrostatic pressure

Samy Mansy

s.mansy@cst.ps

University College of Science and Technology – Khan Younis https://orcid.org/0009-0007-2805-5715

Research Article

Keywords: Cadmium Telluride (CdTe), Hydrostatic pressure, Band gap tuning, CASTEP, DFT, Phonon dynamics, Thermodynamic properties, Raman spectroscopy, High-pressure behavior

Posted Date: April 14th, 2026

DOI: https://doi.org/10.21203/rs.3.rs-9398987/v1

License: This work is licensed under a Creative Commons Attribution 4.0 International License.
Read Full License

Additional Declarations: The authors declare no competing interests.

First-principles investigation of pressure-dependent structural, electronic, vibrational, and thermodynamic properties of zinc-blende CdTe under hydrostatic pressure

Mansy Samy

University College of Science and Technology – Khan Younis, Department of Engineering Sciences and Applied Arts. Gaza, Palestine.

s.mansy@cst.ps

Abstract

This study presents a comprehensive first-principles investigation of the structural, electronic, vibrational, and thermodynamic properties of zinc-blende (ZB) CdTe under hydrostatic pressure up to 50 GPa, using density functional theory (DFT) within the PBE-GGA framework as implemented in the CASTEP code. Cadmium telluride (CdTe) is a technologically important semiconductor widely used in thin-film photovoltaic devices, where CdTe-based solar cells have achieved conversion efficiencies of approximately 22%. The structural analysis reveals a monotonic reduction in the lattice parameter and unit cell volume with increasing pressure, confirming isotropic compression behavior consistent with the Birch-Murnaghan equation of state. The electronic band gap exhibits a pronounced non-monotonic pressure dependence, increasing from 1.59 eV at ambient pressure to a maximum of 2.22 eV at approximately 20 GPa, followed by a decrease to 1.63 eV at 50 GPa. This behavior is attributed to pressure-induced orbital redistribution and modifications at the band edges, primarily involving Te-5p and Cd-5s states, as elucidated by density of states (DOS) analysis. Vibrational properties, analyzed through Raman spectra, show a continuous blueshift in phonon wavenumbers with pressure, indicating bond stiffening and increased interatomic force constants, accompanied by significant variations in spectral intensity due to anharmonic effects. The thermodynamic response, including enthalpy, Gibbs free energy, heat capacity, and Debye temperature, demonstrates strong pressure sensitivity, reflecting modified lattice dynamics and reduced thermodynamic stability under compression. It is important to note that calculations beyond approximately 20 GPa were performed under constrained zinc-blende symmetry to explore property trends and should be interpreted as indicative of metastable behavior. The results establish CdTe as a pressure-tunable semiconductor and identify ~20 GPa as a significant threshold for changes in its electronic and vibrational behavior, providing a valuable reference for future experimental and theoretical studies on CdTe under extreme conditions.

Keywords: Cadmium Telluride (CdTe); Hydrostatic pressure; Band gap tuning; CASTEP ; DFT; Phonon dynamics; Thermodynamic properties; Raman spectroscopy; High-pressure behavior.

I. Introduction

Cadmium telluride (CdTe) is a technologically important II–VI semiconductor that crystallizes in the zinc-blende (ZB) cubic structure under ambient conditions and possesses a direct band gap of approximately 1.5–1.6 eV, which is close to the optimal value for solar energy conversion [1]. Owing to its high optical absorption coefficient, suitable band gap, and favorable carrier transport properties, CdTe has become one of the most widely used materials in thin-film photovoltaic technology. In particular, CdTe-based solar cells have achieved power conversion efficiencies approaching 22%, highlighting the technological significance of this material in modern renewable energy systems [1]. Beyond photovoltaics, CdTe is also employed in radiation detectors, infrared optics, and various optoelectronic devices due to its advantageous electronic and structural characteristics.

Investigating the response of CdTe to external pressure is of considerable scientific interest because pressure provides a clean and controllable means of tuning interatomic distances and electronic interactions without introducing chemical disorder. Hydrostatic compression can significantly influence lattice parameters, orbital hybridization, and lattice dynamics, thereby modifying electronic band structures, phonon spectra, and thermodynamic properties. Consequently, high-pressure studies have become a powerful approach for understanding the fundamental physical behavior of semiconductors and for exploring potential routes to engineer their functional properties [2].

Previous experimental and theoretical studies have shown that CdTe undergoes pressure-induced structural transformations. In particular, the zinc-blende (B3) phase transforms into the rock-salt (B1) structure under sufficiently high compression, reflecting the sensitivity of the Cd–Te bonding environment to external stress [3]. Such structural changes are typically accompanied by significant modifications in the electronic structure, including variations in band ordering, band gap magnitude, and hybridization between Cd-5s and Te-5p states near the band edges.

In addition to structural and electronic effects, the vibrational and thermodynamic properties of CdTe under pressure are essential for understanding its stability and lattice dynamics. External pressure can strongly affect phonon frequencies, Raman spectra, and thermodynamic quantities such as enthalpy, heat capacity, and Debye temperature, providing valuable insights into lattice stiffness and the dynamical behavior of the crystal under extreme conditions [7].

Although numerous studies have investigated specific aspects of CdTe, such as its electronic structure or vibrational properties, a comprehensive investigation that simultaneously examines structural, electronic, vibrational, and thermodynamic responses under hydrostatic pressure remains relatively limited. Such an integrated analysis is necessary for clarifying the interplay between these physical properties and for developing a consistent theoretical description of pressure-induced behavior in this technologically important semiconductor [8].

In this work, we present a systematic first-principles investigation of zinc-blende CdTe under hydrostatic pressures up to 50 GPa using density functional theory (DFT) within the generalized gradient approximation (PBE-GGA), as implemented in the CASTEP computational package [6]. The evolution of structural parameters, electronic band structure, density of states, vibrational characteristics, and thermodynamic properties is analyzed in detail. Although CdTe is known to undergo a pressure-induced transition from the zinc-blende (B3) phase to the rock-salt (B1) phase at relatively low pressures, the present study intentionally focuses on the metastable continuation of the zinc-blende structure. By constraining the calculations within the ZB symmetry, we aim to isolate the intrinsic pressure-dependent evolution of its physical properties independently of structural phase transitions. The results provide a comprehensive theoretical perspective on the pressure-tunable properties of CdTe and offer useful guidance for future experimental studies and advanced optoelectronic applications operating under high-pressure conditions.

2. METHODS OF CALCULATION

The present study was carried out using first-principles calculations based on density functional theory (DFT), as implemented in the CASTEP simulation package [8–9]. Exchange–correlation effects were treated within the generalized gradient approximation (GGA) using the Perdew–Burke–Ernzerhof (PBE) functional, which generally provides improved structural and electronic predictions compared with the local density approximation (LDA) [10]. Structural optimization was performed by minimizing the total energy and interatomic forces using the following convergence thresholds: 1×10^{-5} eV/atom for total energy, 0.0003 eV/Å for maximum force, 0.0001 GPa for maximum stress, and 2×10^{-4} Å for maximum atomic displacement.

Brillouin-zone sampling was carried out using a Monkhorst–Pack k-point mesh of $6 \times 6 \times 6$. A plane-wave cutoff energy of 500 eV was adopted, and norm-conserving pseudopotentials were used to describe the core–valence electron interactions for Cd and Te. The valence electronic configurations considered for the pseudopotentials were Cd: $4d^{10}5s^2$ and Te: $5s^25p^4$. All calculations were performed on the primitive unit cell of zinc-blende CdTe (space group F-43m).

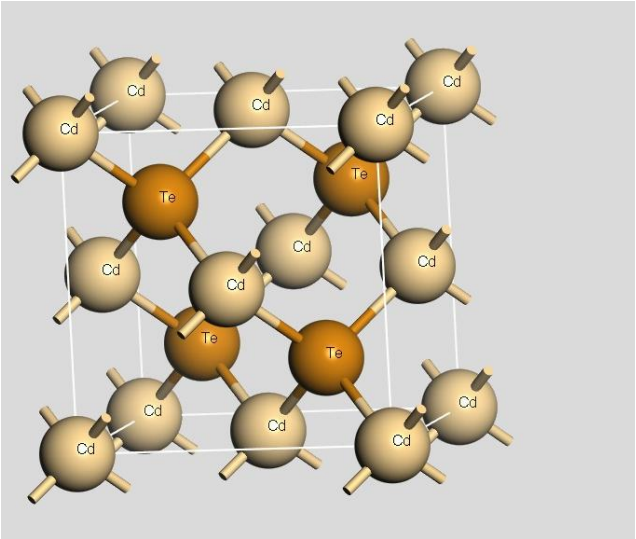


Fig. 1 – Primitive unit cell of the zincblende (cubic) CdTe structure.

3. RESULTS AND DISCUSSION

The structural response of cubic CdTe to hydrostatic pressure was investigated via simulated XRD patterns at 0, 20, and 50 GPa. A systematic shift in diffraction peaks toward higher 2θ angles was observed, consistent with Bragg's law, indicating a decrease in interplanar spacing d due to lattice compression [11]. The distance between crystallographic planes, related to the cubic lattice constant by :

$$d_{hkl}=\frac{a}{\sqrt{h^2+k^2+l^2}} \qquad (1)$$

showed a measurable reduction, confirming isotropic lattice shrinkage [12]. Accordingly, the unit cell volume (a3) decreased with pressure, while maintaining cubic symmetry [13]. The pressure-induced volumetric response correlates with the Murnaghan equation of state :

$$P(V)=B\left[1-B'\left(\frac{\Delta V}{V}\right)\right] \qquad (2)$$

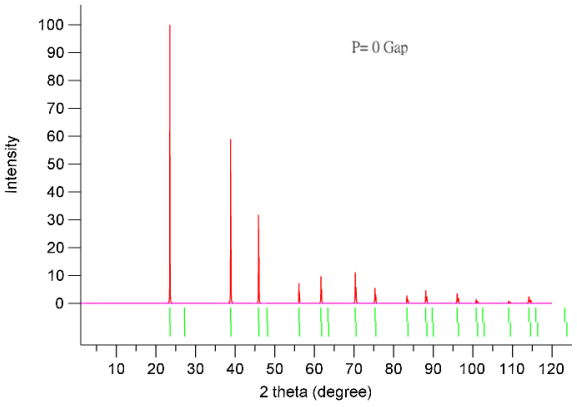
supporting the observed densification trend [14]. These results demonstrate CdTe's robustness under pressure and validate the accuracy of DFT-based predictions for crystallographic behavior. The findings align with prior reports on II–VI semiconductors, confirming pressure-induced lattice stiffening without structural breakdown [15].

3.1 Structural and Crystallographic Characterization

The calculated X-ray diffraction (XRD) patterns for cubic CdTe at pressures of 0, 20, and 50 GPa reveal a systematic shift of the diffraction peaks toward higher 2θ angles as pressure increases. According to Bragg's law, this shift indicates a progressive reduction in the interplanar spacing (d), reflecting lattice contraction under hydrostatic compression. The preservation of the characteristic peak sequence and the absence of additional reflections indicate that the zinc-blende (ZB) structure remains preserved within the applied simulation conditions. The observed peak displacement is associated with a decrease in the lattice parameter (a) and a corresponding increase in crystal density, with the most pronounced compression occurring at 50 GPa, suggesting enhanced atomic packing and structural compaction.

It should be emphasized that these XRD patterns were obtained from geometry optimizations performed under constrained ZB symmetry at each pressure. Consequently, the absence of new diffraction peaks mainly reflects isotropic compression within this structural framework and does not necessarily imply thermodynamic phase stability up to 50 GPa. Interestingly, the non-monotonic evolution of the electronic band gap near 20 GPa (discussed in Section 3.3), together with noticeable variations in the pressure dependence of vibrational and thermodynamic properties, suggests that this pressure region may represent a precursor to structural instability or a potential phase transition.

Therefore, results obtained at pressures above approximately 20 GPa should be interpreted cautiously as representing the metastable continuation of the ZB phase under the imposed symmetry constraints. The present approach aims to isolate intrinsic pressure-induced trends in the structural, electronic, vibrational, and thermodynamic properties of CdTe without the influence of structural phase transformations. A definitive determination of the stable high-pressure phase would require additional investigations, including enthalpy comparisons and phonon dispersion analyses.



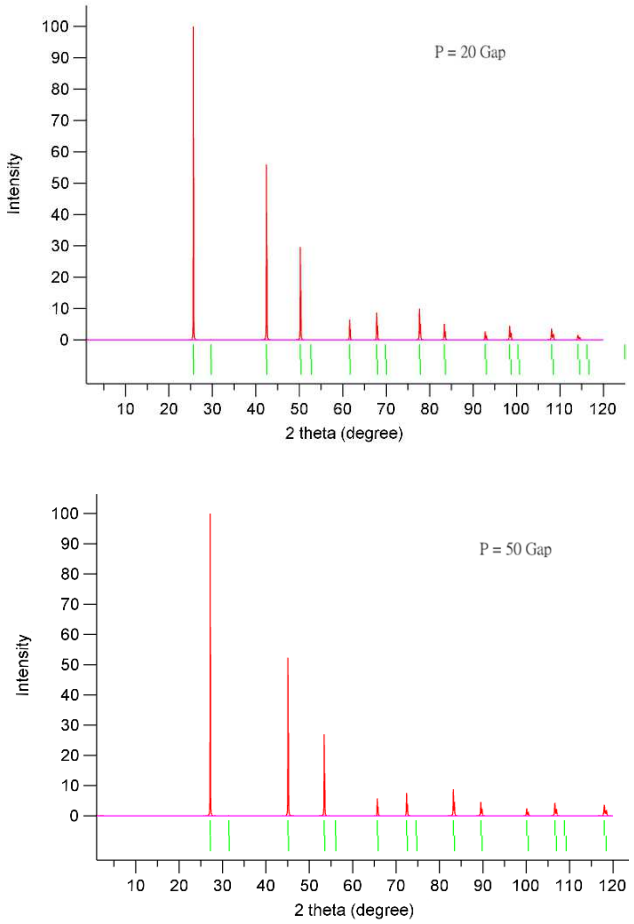


Fig. 2 – Plot of computational XRD patterns of cubic CdTe under Pressure

3.2 Density of States (DOS) :

The calculated total and partial density of states (TDOS/PDOS) of CdTe under hydrostatic pressures exhibits pronounced broadening and peak splitting, particularly near the band edges, indicating pressure-induced modifications in bonding characteristics and a redistribution of Te-5p and Cd-5s states [16]. This behavior reflects enhanced orbital overlap and hybridization under compression, which strongly influences the electronic configuration of CdTe.

Consistently, the electronic band structure shown in Fig. 4 along the high-symmetry directions of the Brillouin zone (W, L, Γ, X, K) supports this trend, revealing a progressive departure from the typical direct bandgap nature at low pressure toward an altered electronic configuration at higher pressure. Such electronic changes are in agreement with theoretical predictions suggesting proximity to phase-transition thresholds near 50 GPa [9]. Furthermore, Fig. 5 summarizes the pressure dependence of the band gap, showing a clear increase up to 20 GPa, followed by a reduction at higher pressures. This non-monotonic behavior implies complex pressure-driven electronic rearrangements, which may involve band hybridization and/or structural distortions [17–18].

Consequently, the pressure-dependent evolution of DOS and band dispersion highlights CdTe as a promising candidate for pressure-adaptive optoelectronic applications, including pressure-sensitive photodetectors, sensors, and tunable photovoltaic devices, particularly for harsh-environment operation [17–18]. The distinct electronic modifications observed in both the DOS and band structure further emphasize the feasibility of engineering energy devices tailored to specific pressure regimes, in accordance with previous experimental and theoretical reports [19]. In addition, the bandgap variation extracted from the TDOS (shown in the inset at the top-right of the corresponding figure) can be attributed to the increased orbital overlapping between tellurium **[Te] $4d^{10}$ $5s^2$ $5p^4$** and cadmium **[Cd] $4d^{10}$ $5s^2$** electronic configurations under pressure, which alters band ordering and controls the bandgap evolution [16].

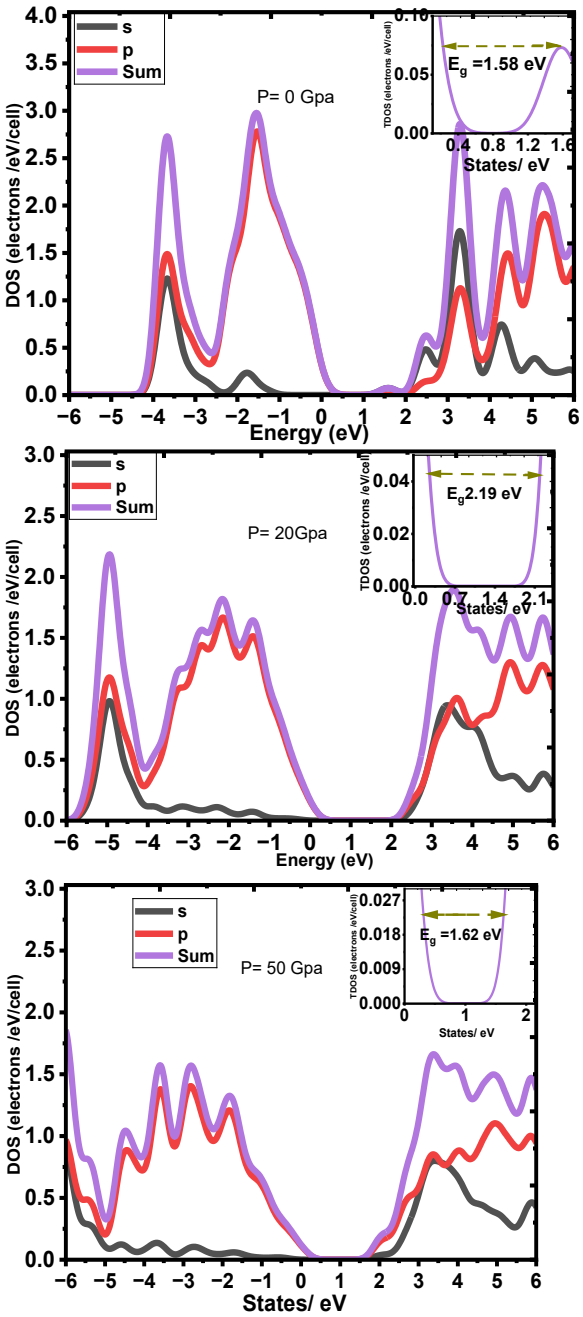
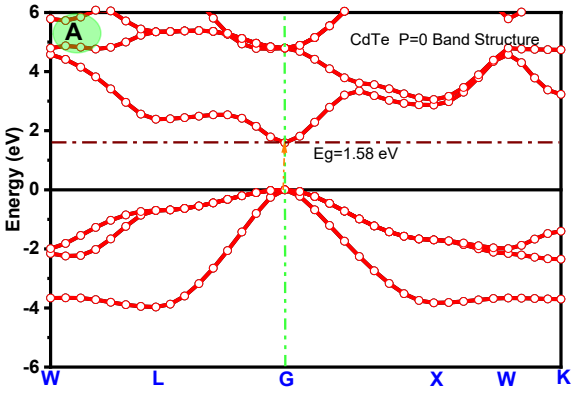


Fig. 3 – Partial and total density of state of CdTe

under pressure.

3.3 Band structure evolution of CdTe under different hydrostatic pressure :

The electronic and optical response of cadmium telluride (CdTe) under hydrostatic pressure provides valuable insight into its pressure-tunable semiconducting behavior. Fig. 4 presents the calculated electronic band structures along the high-symmetry directions of the Brillouin zone for pressures ranging from 0 to 50 GPa, where the Fermi level is set to zero energy (horizontal black line). It should be noted that density functional theory within the PBE-GGA approximation generally underestimates semiconductor band gaps. However, the calculated value in the present work remains in reasonable agreement with available experimental and theoretical data for CdTe. At ambient pressure (0 GPa), CdTe crystallizes in the zinc-blende structure and exhibits a direct bandgap of 1.58 eV at the Γ point. The valence band maximum (VBM) is mainly dominated by Te-5p states, whereas the conduction band minimum (CBM) is primarily contributed by Cd-5s states [20–21]. As the pressure increases up to 20 GPa, the bandgap increases nearly linearly to 2.194 eV, which can be attributed to the upward shift of the conduction band edge (mainly s-like states) occurring more rapidly than the valence band edge (p-like states) [3]. At this pressure range, the electronic band ordering is modified and the bandgap may evolve toward an indirect character, consistent with earlier reports [22]. Upon further compression to 50 GPa, the bandgap decreases to 1.63 eV, indicating a non-monotonic pressure dependence. This behavior suggests pressure-driven electronic rearrangements that may involve enhanced band hybridization and/or pressure-induced structural distortions [23]. The overall pressure dependence of the bandgap is summarized in Fig. 5.



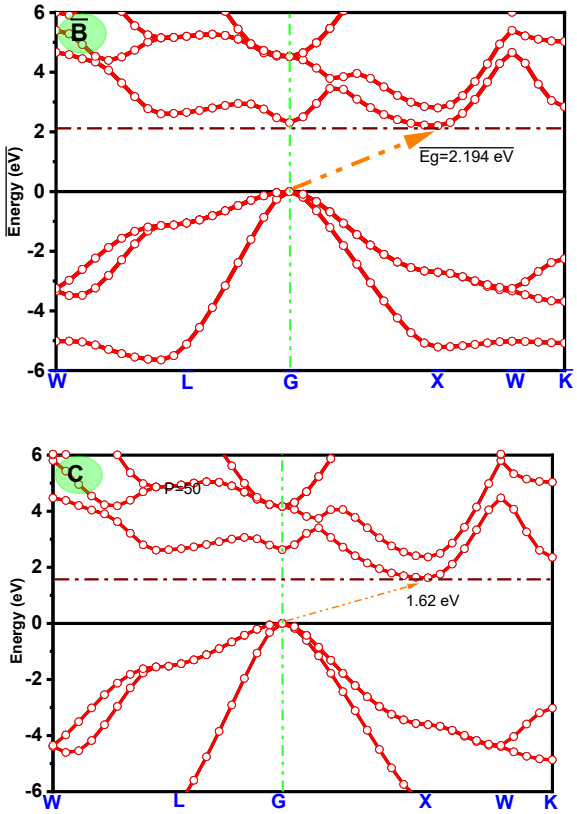


Fig. 4 – Calculated electronic band structure along the high-symmetry directions in the Brillouin zone, under the influence of different pressures.

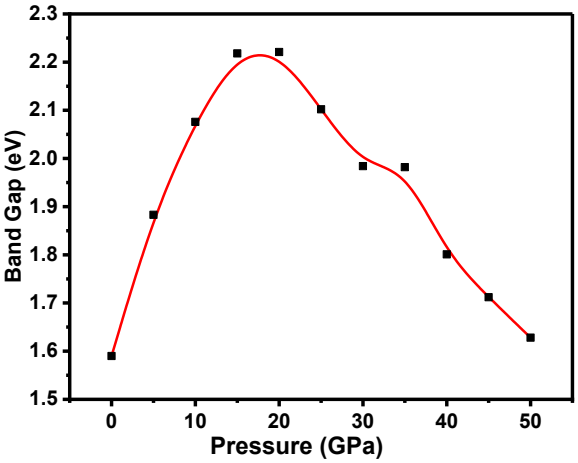


Fig. 5 – Pressure **dependence of band gap in CdTe**

3.4 Phonon Properties and Lattice Vibrations

The calculated phonon dispersion of zinc-blende CdTe along the high-symmetry directions of the Brillouin zone is shown in Fig. 6.1. As expected for a primitive cell containing two atoms, the phonon spectrum consists of six branches, including three acoustic modes and three optical modes. The acoustic branches originate from the Γ point and approach zero frequency, which is consistent with the translational invariance of

the crystal lattice, while the optical branches are located at higher frequencies, extending approximately from 3.6 to 5.0 THz. The acoustic modes are mainly distributed below about 1.8 THz, indicating a clear separation between low-frequency lattice vibrations and high-frequency optical excitations. Overall, the absence of negative phonon frequencies in the calculated dispersion supports the dynamical stability of the zinc-blende CdTe structure within the present computational conditions. Since phonon modes govern lattice vibrations, thermal response, and vibrational spectroscopy, the phonon dispersion shown in Fig. 6.1 provides the fundamental basis for interpreting the pressure-dependent Raman shifts, vibrational behavior, and thermodynamic properties discussed in the following sections[61],[62] .

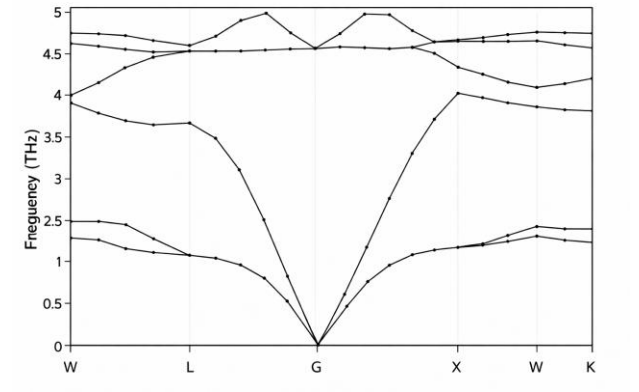


Fig. 6.1– Phonon dispersion curves of zinc-blende CdTe along the high-symmetry directions of the Brillouin zone (W–L–Γ–X–W–K).

لاحظ انه هذا عند 0 **gap**

3.5 Pressure dependence of wave number and intensity:

The vibrational response of CdTe under applied pressure shows clear variations in both spectral intensity and phonon wavenumber. As illustrated in Fig. 6.3, the spectral intensity decreases nonlinearly with increasing pressure, dropping from approximately 77.98 km/mol at 0 GPa to about 39.96 km/mol at 50 GPa. This behavior can be described by an exponential relation: $I(P) = I_0 \exp(-\beta P)$, where I_0 represents the initial intensity, and β denotes the pressure sensitivity associated with dipole-moment variations [24]. This trend suggests that compression induces distortions in the Cd–Te bonding environment, which may be enhanced by anharmonic effects and electron–phonon coupling, leading to changes in vibrational symmetry and transition strength [25]. In contrast, the phonon wavenumber increases with pressure, as shown in Fig. 6.2, shifting toward higher values (blueshift). This blueshift indicates bond stiffening and an increase in the effective force constants under high-pressure conditions [26].

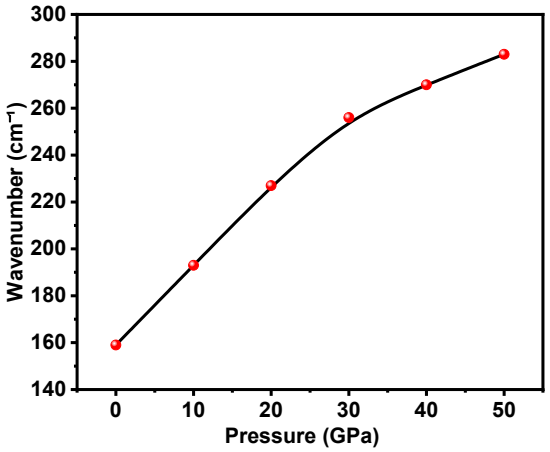


Fig. 6.2 – Pressure dependence of the phonon wavenumber in CdTe under hydrostatic compression (0–50 GPa).

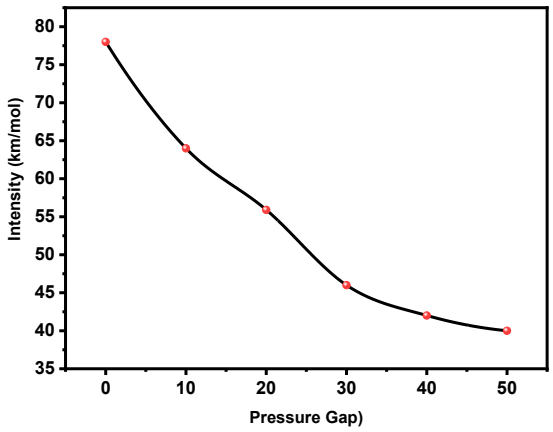


Fig. 6.3 – Pressure dependence of the spectral intensity in CdTe under hydrostatic compression (0–50 GPa).

4. Mechanical Properties

4.1 The Lattice parameter against external pressure

Fig. 7 shows the pressure dependence of the cubic lattice parameter (a = b = c) of CdTe up to 50 GPa. The lattice constant decreases nearly linearly with increasing pressure, reflecting the expected elastic compression of the crystal lattice [27]. Specifically, the lattice parameter is reduced from about 6.62 Å at 0 GPa to approximately 5.592 Å at 50 GPa, corresponding to a relative contraction of ~ 15.50 %. The calculated equilibrium lattice constant at 0 GPa (6.6201 Å) agrees well with the experimental values reported in the literature [28–29]. In the low-pressure region (0–~20 GPa), the trend remains smooth without pronounced anomalies, suggesting that CdTe retains its cubic symmetry within this range in the present zinc-blende–constrained calculations. At higher pressures approaching 50 GPa, the enhanced contraction may indicate proximity to a pressure-induced structural transformation; however, confirming a phase transition requires additional structural or thermodynamic analysis [28].

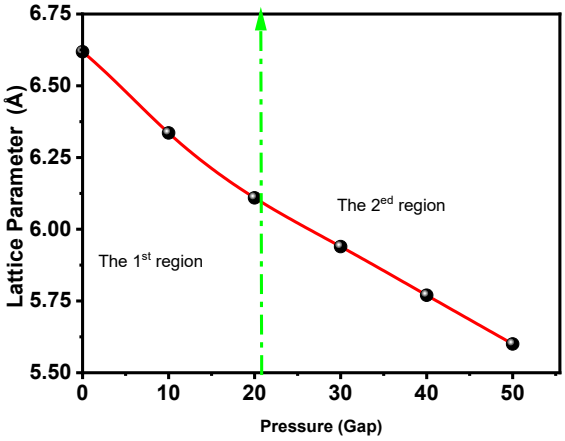


Fig. 7 – Behavior of contraction of lattice parameter Vs applied pressure in CdTe

4.2 Comparison of calculated structural and electronic properties of CdTe with previous studies.

Table 2 : presents a comparison between the calculated structural and electronic properties obtained in the present work and previously reported theoretical and experimental values. The calculated lattice constant of CdTe (6.62 Å) agrees well with previously reported values in the range of 6.48–6.62 Å. Similarly, the calculated band gap of 1.58 eV is consistent with earlier theoretical predictions considering the well-known band gap underestimation in PBE-GGA calculations. The obtained bulk modulus (~45 GPa) also falls within the reported range of 42–50 GPa. This good agreement confirms the reliability of the computational parameters used in the present study.

Table 2. Comparison of calculated structural and electronic properties of CdTe with previous studies.

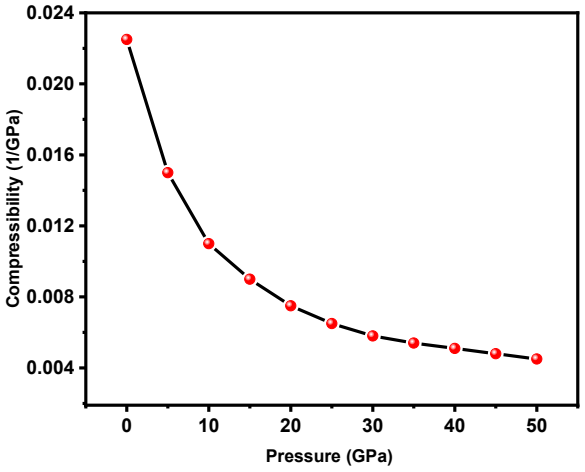
Property	Present Work	Literature	Reference
Lattice constant (Å)	6.620	6.48 – 6.62	Wei & Zhang (2000)[58]
Band gap (eV)	1.58	~1.50	Gupta & Bansil (2003)[59]
Bulk modulus (GPa)	44.99	42 – 50	Wang et al. (2005)[60]

4.3 Pressure-dependent behaviour of compressibility (K) and the bulk modulus (B)

As shown in Fig. 8, the compressibility (κ) of CdTe decreases markedly with increasing pressure, dropping from approximately 0.0225 GPa^{-1} at 0 GPa to about 0.0050 GPa^{-1} at 50 GPa, which is consistent with the expected reduction in lattice compressibility under hydrostatic compression [32]. This pressure dependence can be described using an exponential fitting relation:

$$\kappa(P) = \kappa_0 \cdot \exp(-P/\beta) \qquad (3)$$

where κ_0 represents the initial compressibility and β denotes the pressure sensitivity parameter associated with the resistance of the lattice to volume reduction [30]. Correspondingly, the bulk modulus (B) increases significantly over the same pressure range (from ~44.99 GPa up to ~222 GPa), confirming progressive volumetric stiffening and enhanced resistance to compression [31]. The rapid decrease in κ at low pressures may be attributed to early bond-length adjustment and enhanced interatomic interactions, whereas the more gradual decrease at higher pressures reflects increasing electron-density overlap and stronger repulsive forces under compression [31]. Overall, the evolution of B with pressure is in good agreement with the typical behavior predicted by the Birch–Murnaghan equation of state, supporting the mechanical stiffening of CdTe under high-pressure conditions [32].



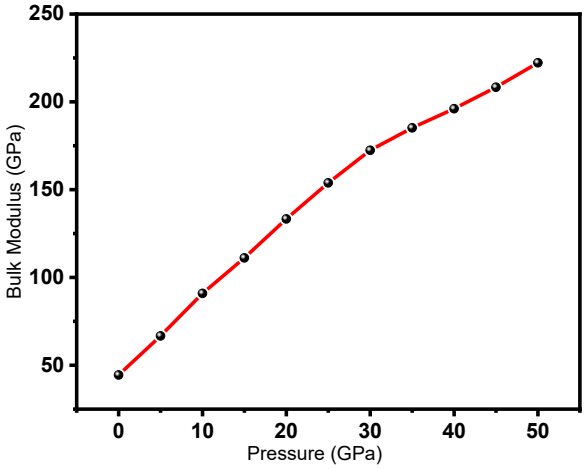


Fig. 8 –Pressure-dependent behavior of compressibility and bulk modulus in CdTe.

5 . Raman spectrum of CdTe under different pressures :

The Raman spectra of CdTe exhibit clear pressure-dependent variations in both peak position and intensity, reflecting changes in lattice dynamics and interatomic interactions under compression (Fig.9). It should be noted that the intensity discussed in Section 3.4 refers to the IR (spectral) intensity expressed in km/mol, whereas the Raman intensity reported here represents a normalized Raman scattering intensity (Δμ/Aμ); therefore, the different pressure-dependent trends of these two quantities are expected and do not indicate any inconsistency. At ambient pressure (0 GPa), a pronounced Raman peak appears near 150 cm^{-1} with an intensity of about 0.014 (Δμ/Aμ), which is consistent with the characteristic vibrational response of cubic zinc-blende CdTe, alongside a bandgap of approximately 1.59 eV [46]. Upon increasing the pressure to 20 GPa, the Raman peak shifts to higher wavenumber (≈220 cm^{-1}) while the intensity decreases to around 0.01, accompanied by an expansion of the bandgap to 2.194 eV [32]. This blueshift is attributed to reduced interatomic distances and enhanced bond stiffness under compression, which increase the restoring forces associated with lattice vibrations [3]. At 50 GPa, the Raman mode further shifts to approximately 260 cm^{-1}, indicating continued phonon hardening, whereas the intensity increases markedly to about 0.09. Such intensity changes may arise from pressure-induced modifications in polarizability and Raman scattering efficiency, potentially linked to symmetry variations and enhanced electron–phonon interactions at high pressure [32, 48]. Meanwhile, the reduction of the bandgap to 1.63 eV at 50 GPa suggests pressure-driven electronic reconfiguration and may indicate that CdTe approaches a regime of structural instability; however, confirming a pressure-induced phase transition requires additional thermodynamic analysis or experimental structural validation [46–47, 49]. Overall, these results highlight the strong pressure-tunable vibrational response of CdTe, supporting its relevance for high-pressure optoelectronic and sensing applications [49]. It is important to note that the analysis at higher pressures is discussed within a ZB-constrained framework; therefore, trends above ~20 GPa should be interpreted cautiously as a metastable continuation of the ZB phase.

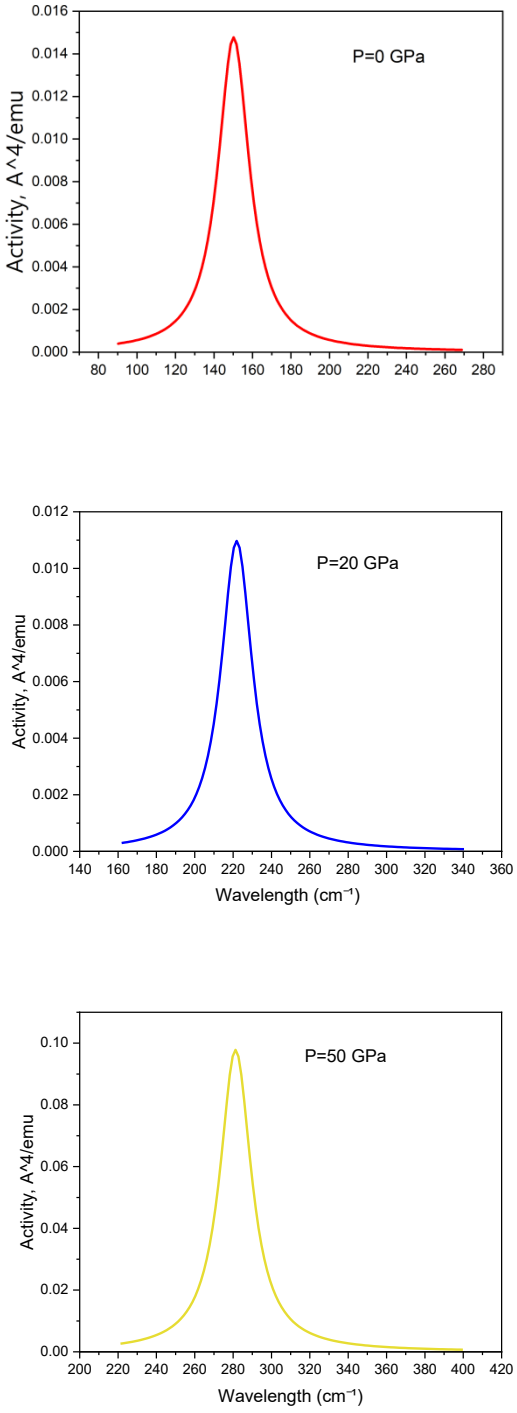


Fig. 9 - Raman spectrum of CdTe under different pressures

6. Thermodynamic properties :

In order to gain a comprehensive understanding of phonon properties, the thermodynamic enthalpy H, the free energy G and the entropy S at finite temperature can be computed. The thermodynamic response of CdTe under various pressure conditions (0, 20, and 50 GPa) demonstrates clear dependencies of its stability and heat capacity on external stress.

6.1 Temperature-dependent behavior of enthalpy (H) at pressures of 0, 20, and 50 GPa

Fig. 10 presents the calculated enthalpy (H) of CdTe as a function of temperature at pressures of 0, 20, and 50 GPa. In all cases, H increases monotonically with temperature, reflecting the continuous accumulation of thermal energy due to lattice vibrations. At 0 GPa, the enthalpy rises from nearly zero at low temperatures to about 0.47–0.48 eV at 1000 K, while lower values are observed under pressure, reaching approximately 0.22 eV at 20 GPa and 0.28–0.30 eV at 50 GPa at the same temperature. At low temperatures, the enthalpy curves exhibit noticeable curvature due to anharmonic lattice contributions. Above approximately 50–60 K, the curves become nearly linear, indicating that the heat capacity approaches an almost constant value. The reduced enthalpy under compression suggests enhanced lattice stability and suppressed thermal fluctuations. The smooth behavior indicates that no abrupt thermodynamic anomaly is observed within the assumed zinc-blende configuration over the considered temperature range. However, this does not by itself establish phase stability against competing high-pressure structures; the observed non-monotonic behavior of the electronic band gap around 20 GPa (discussed in Section 3.3), combined with changes in vibrational and thermodynamic properties, suggests this pressure range as a potential region of instability. Therefore, results beyond approximately 20 GPa should be interpreted cautiously as a constrained/metastable continuation rather than an equilibrium phase [41, 56–57].

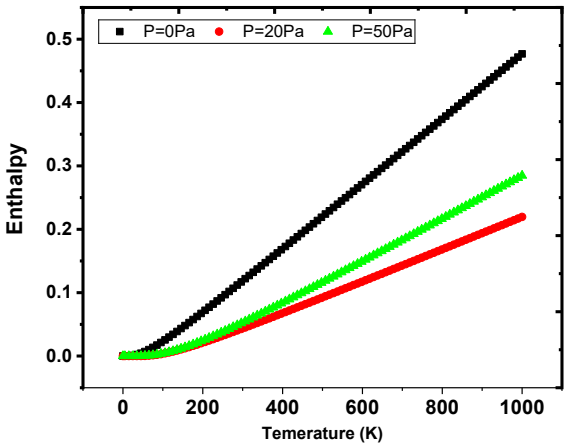


Fig. 10 –Temperature-dependent behavior of enthalpy (**Й)** at three different pressure cases.

6.2 Pressure-dependent Gibbs free energy of cubic CdTe

As depicted in Fig. 11, the Gibbs free energy G, which governs thermodynamic phase stability, is defined as

$$G = H - TS \qquad (4)$$

where H is the enthalpy (H = U + PV), S is the entropy, and T is the absolute temperature (K). Fig. 11 shows the temperature dependence of G for cubic CdTe at three pressures (0, 20, and 50 GPa). In all cases, G(T) remains negative over the investigated temperature range and exhibits a concave-down curvature, consistent with the thermodynamic condition

$$(\partial^2 G/\partial T^2)_P < 0 \qquad (5)$$

The negative slope $(\partial G/\partial T)_P$ indicates positive entropy

$$S = -(\partial G/\partial T)_P \qquad (6)$$

while the downward curvature reflects a positive heat capacity. At ambient pressure (0 GPa), CdTe displays the lowest values of G, indicating the highest thermodynamic stability among the examined pressure states. With increasing pressure, G becomes less negative, reflecting pressure-induced changes in the balance of enthalpic and entropic contributions and suggesting a reduced thermodynamic driving tendency for stability of the cubic phase under compression [4]. In addition to enthalpy and Gibbs free energy, the thermal response of CdTe is further examined through its heat capacity and Debye temperature as functions of pressure and temperature.

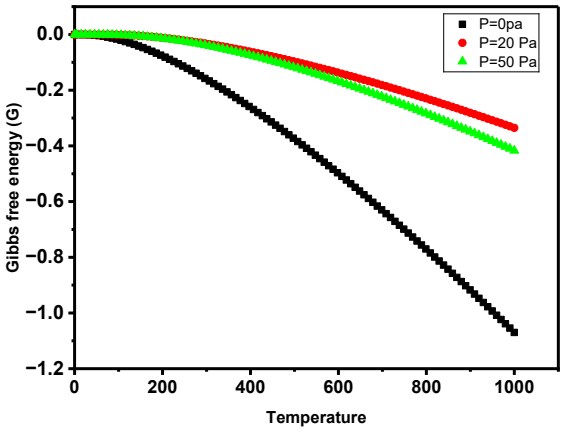


Fig. 11 –Temperature-dependent behavior of Gibbs free energy (Ğ) at three different pressure cases.

6.3 Pressure-Dependent Heat Capacity of Cubic CdTe

Fig. 12 shows the temperature dependence of the constant-volume heat capacity (Cv) of cubic CdTe under different hydrostatic pressures. In all cases, Cv increases rapidly at low temperatures due to the gradual activation of phonon modes, then rises more slowly and approaches a saturation behavior at higher temperatures, consistent with the classical Dulong–Petit limit. At ambient pressure (0 GPa), Cv reaches approximately 11.5–12.0 $J \cdot mol^{-1} \cdot K^{-1}$ at high temperatures, reflecting the full contribution of lattice vibrations. Under compression, the heat-capacity values are reduced, where Cv decreases to about 5.5–6.0 $J \cdot mol^{-1} \cdot K^{-1}$ at 20 GPa, and becomes ap-

proximately 7.5–8.0 J·mol⁻¹·K⁻¹ at 50 GPa. This reduction indicates that hydrostatic pressure suppresses vibrational contributions by stiffening the lattice and shifting phonon frequencies, thereby limiting the thermal population of vibrational states. Within the Debye model, the constant-volume heat capacity can be expressed as:

$$C_v(T)=9NK_B\int_0^{\frac{\Theta D}{T}}\frac{x4\ e^x}{(e^x-1)2}dx \qquad (7)$$

where N is the number of atoms, kB is the Boltzmann constant, and ΘD is the Debye temperature. Overall, the pressure-dependent evolution of Cv provides additional insight into the modified lattice dynamics of CdTe and supports its thermodynamic behavior under high-pressure conditions [52-53-54].

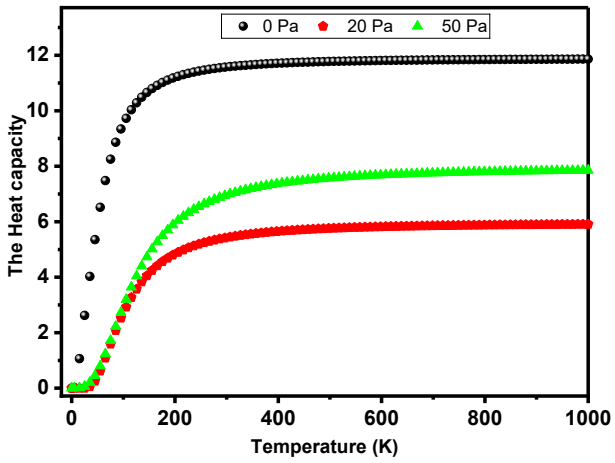


Fig. 12 – Temperature dependence of the heat capacity (Cv) of CdTe at 0, 20, and 50 GPa

6.4 Temperature and Pressure Dependence of the Debye Temperature of Cubic CdTe

It should be noted that the pressure dependence of the Debye temperature may exhibit complex behavior at low temperatures due to the dominant contribution of acoustic phonon modes and anharmonic lattice effects. Consequently, small variations in ΘD with pressure in this regime do not necessarily contradict the general trend of lattice stiffening under compression. It is worth noting that the pressure dependence of the Debye temperature is temperature-sensitive: at low temperatures, ΘD decreases with pressure, whereas at higher temperatures it exhibits an increasing trend with pressure, consistent with the calculated data. In Fig. 13, the Debye temperature of cubic CdTe is presented as a function of both temperature and external pressure, showing significant variations across different thermal regimes. The pronounced decrease of ΘD at low temperatures (T < 100 K) is primarily attributed to the dominance of low-frequency acoustic phonons. Under zero pressure, the Debye temperature of cubic CdTe lies in the range of 210–220 K. Upon applying pressure, ΘD decreases to approximately 170–180 K at 20 GPa and further to about 140–150 K at 50 GPa, indicating a softening behavior within the low-temperature regime where acoustic contributions remain dominant.

In contrast, ΘD increases with temperature at all pressures; however, its dependence on pressure changes with temperature. For example, at 300 K, the Debye temperature is approximately 230 K at 0 GPa, increases to about 250 K at 20 GPa, and reaches nearly 270 K at 50 GPa, with this trend continuing as temperature rises. Similarly, at 1000 K, ΘD is about 310–320 K at 0 GPa, increases to at least 330 K at 20 GPa, and reaches approximately 340–350 K at 50 GPa. This high-temperature increase of ΘD with pressure suggests enhanced lattice stiffening under compression and stronger interatomic interactions, leading to reduced vibrational amplitudes and improved thermal stability of cubic CdTe [50-51-55].

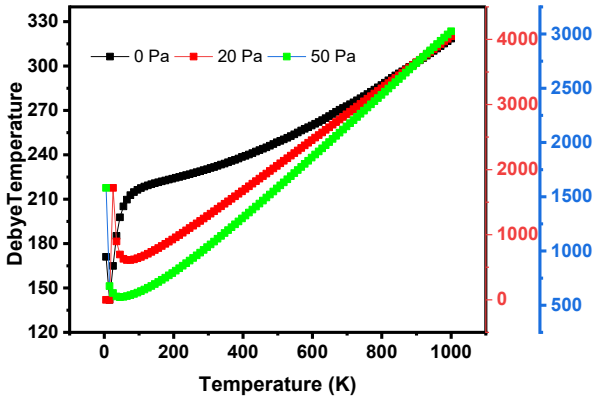


Fig. 13 –Temperature-dependent variation of the Debye temperature of cubic CdTe under different applied pressures.

7. Conclusion:

This work presents a comprehensive first-principles investigation of the structural, electronic, vibrational, and thermodynamic properties of zinc-blende (ZB) CdTe under hydrostatic pressures up to 50 GPa within the PBE-GGA framework of density functional theory. The structural analysis reveals a monotonic decrease in the lattice parameter with increasing pressure, consistent with isotropic compression and well described by the Birch–Murnaghan equation of state. Correspondingly, the bulk modulus increases significantly, indicating enhanced lattice stiffness and .resistance to compression

The electronic properties exhibit a pronounced non-monotonic pressure dependence of the band gap. The

band gap increases from 1.59 eV at ambient pressure to a maximum value of about 2.22 eV near 20 GPa, followed by a gradual decrease to approximately 1.63 eV at 50 GPa. This behavior is mainly attributed to pressure-induced modifications in the electronic band edges associated with hybridization between Te-5p and .Cd-5s states, as confirmed by density of states analysis

The vibrational response shows a systematic blueshift in phonon frequencies with increasing pressure, indicating bond stiffening and enhanced interatomic force constants. In parallel, thermodynamic quantities including enthalpy, Gibbs free energy, heat capacity, and Debye temperature display a strong pressure dependence, reflecting substantial modifications in .lattice dynamics under compression

It should be emphasized that calculations above approximately 20 GPa were performed under constrained zinc-blende symmetry. Therefore, the results in this region should be interpreted as representing a metastable continuation of the ZB phase and may indicate proximity to a pressure-induced .structural transition

Overall, the present results identify CdTe as a pressure-tunable semiconductor exhibiting significant electronic and vibrational modifications around ~20 GPa. These findings provide a consistent theoretical framework for understanding pressure-induced behavior in CdTe and related II–VI semiconductors. Future work may include a detailed investigation of the B3–B1 phase transition through enthalpy comparisons and phonon dispersion calculations in order to determine the thermodynamically stable high-pressure .phase

Acknowledgments

The author would like to acknowledge the support provided by the Department of Physics, University College of Science and Technology, Khan Younis, Palestine. The computational resources used in this .work are also gratefully acknowledged

Conflict of Interest

The author declares that there are no known competing financial interests or personal relationships that could have appeared to influence the work reported in this .paper

Data Availability

The data that support the findings of this study are available from the corresponding author upon .reasonable request

REFERENCES

1. M. Balkanski, J. Lumin. 7, 451 (1973).
2. J. Jiang, Y. Wang, Y. Zhou, L. Jiang, J. Alloys Compd. 615, 263 (2014).
3. D. Liu, J. Feng, M. Tian, Q. Li, R. Sa, Chem. Phys. Lett. 764, 138272 (2021).
4. D. Gupta, A. Bansil, J. Appl. Phys. 94, 3215 (2003).
5. A.P. Alivisatos, T.D. Harris, L.E. Brus, A. Jayaraman, J. Chem. Phys. 89, 5979 (1988).
6. Y. Huang, W. Jie, Z. Gangqiang, Adv. Mater. Res. 534, 192 (2012).
7. H.K. Hieu, N.T. Hong, P.T.M. Hanh, B.K. Benazzouz, Rom. J. Phys. 69, 603 (2024).
8. J. Chadi, Y. Petroff, M. Balkanski, Phys. Rev. B 5, 3058 (1972).
9. F. Segovia-Chaves, H. Vinck-Posada, Physica B 545, 203 (2018).
10. D. Errandonea, High-Pressure Phase Transitions (Springer, Berlin, 2011).
11. J.P. Perdew, K. Burke, M. Ernzerhof, Phys. Rev. Lett. 77, 3865 (1996).
12. A.K.M. Ali, Al-Mustansiriyah J. Sci. 34, 104 (2023).
13. N. Bouarissa, S. Saib, Comput. Condens. Matter 18, e00423 (2018).
14. Ç. Yamçıçier, C. Kürkçü, Z. Merdan, Solid State Sci. 106, 106209 (2020).
15. I.V. Kalitukha et al., Phys. Rev. B 112, 035304 (2025).
16. S.-H. Wei, S.B. Zhang, Phys. Rev. B 62, 6944 (2000).
17. Y. Benkrima et al., Int. J. Comput. Exp. Sci. Eng. 11, (2025).
18. N. Kishore, V. Nagarajan, R. Chandiramouli, Process. Appl. Ceram. 13, 124 (2019).
19. D. Martínez-García et al., Phys. Status Solidi B 211, 461 (1999).
20. A. Ouahab et al., Chalcogenide Lett. 21, 499 (2024).
21. A. Onodera, Rev. Phys. Chem. Jpn. 39, 123 (1969).
22. Y.-C. Lin, Proc. SPIE 9361, 93610M (2015).
23. S. Mansy et al., Mater. Today Commun. 35, 105688 (2023).
24. F. Baira et al., NeuroQuantology 21, 1371 (2023).
25. E. Unsal, R.T. Senger, H. Sahin, J. Mater. Chem. C 5, 12086 (2017).
26. M. Hoesch et al., Phys. Rev. Lett. 110, 207204 (2013).
27. X. Wang et al., Phys. Rev. B 72, 224102 (2005).
28. H.K. Hieu et al., J. Mater. Sci. Eng. 72, 224102 (2023).
29. K. Kabita et al., Mater. Res. Express 3, 015901 (2016).
30. [30] M.J. Mehl et al., Phys. Rev. B 70, 014105 (2004)..
31. S. Alptekin, J. Mol. Model. 19, 421 (2013).
32. M. Côté et al., Phys. Rev. B 55, 13025 (1997).
33. H.A. Ilchuk et al., Phys. Chem. Solid State 23, 261 (2022).
34. K. Zelenska et al., AIP Conf. Proc. 2010, 020011 (2018).
35. P.T.C. Freire et al., Phys. Rev. B 55, 6743 (1997).
36. F.J. Manjón et al., J. Mater. Chem. C 9, 6277 (2021).
37. E. Eissler et al., MRS Proc. 487, 3 (1997).
38. D. Davorskly et al., J. Phys. D Appl. Phys. 57, 145102 (2024).
39. M.R. Talukder et al., Solid State Commun. 115759 (2024).
40. E. Güler, S. Uğur, JOM (2024).
41. A. Adeniyi et al., Phys. Rev. Res. 2, 033072 (2020).
42. F.I.M. Bincy et al., CrystEngComm 27, 4649 (2025).
43. C. Chen et al., Crystals 9, 497 (2019).
44. Y. Cheng et al., Phys. Rev. B 105, 064106 (2022).
45. R. Minikayev et al., Crystals 11, 764 (2021).
46. D.J. Dunstan, K.P. Homewood, Phys. Rev. B 38, 7862 (1988).
47. K. Natarajan et al., Process. Appl. Ceram. 13, 124 (2019).
48. P. Bhardwaj, S. Singh, Open Chem. 10, 964 (2012).

49. S. Gilliland et al., Phys. Status Solidi B 235, 441 (2003).
50. Z. Feng, Phys. Status Solidi B 222, 451 (2000).
51. D.J. Bradley, K.S. Pitzer, J. Phys. Chem. 83, 1910 (1979).
52. E.F. Talantsev, V.V. Chistyakov, Lett. Mater. 14, 262 (2024).
53. S. Ouendadji et al., Comput. Mater. Sci. 50, 1460 (2011).
54. L. Sun et al., J. Alloys Compd. 822, 153646 (2020).
55. I.F. Al Maaitah, E.B. Elkenany, Comput. Condens. Matter 30, e00640 (2022).
56. S. Kumar, V. Sharma, A.S. Verma, Mater. Chem. Phys. 270, 124778 (2021).
57. Y. Zhao, X. Wang, J. Li, Physica B 624, 413418 (2022)
58. S. H. Wei, S. B. Zhang, Phys. Rev. B 62, 6944 (2000).

59. D. Gupta, A. Bansil, J. Appl. Phys. 94, 3215 (2003).

60. X. Wang, et al., Phys. Rev. B 72, 224102 (2005).

61. P.T.C. Freire et al., Phys. Rev. B 55, 6743 (1997). Raman spectroscopy, optical phonons, and pressure-dependent vibrational behavior في CdTe.

62. M. Côté et al., Phys. Rev. B 55, 13025 (1997). lattice dynamics, phonon-related thermodynamic behavior, and pressure effects.

Supplementary Files

This is a list of supplementary files associated with this preprint. Click to download.

- Abstract.docx